

Influence of pre-deformation on age-hardening response and mechanical properties of extruded Mg–6%Zn–1%Mn alloy

Guo-liang SHI¹, Ding-fei ZHANG^{2,3}, Hong-ju ZHANG², Xia-bing ZHAO⁴, Fu-gang QI², Kui ZHANG¹

1. State Key Laboratory for Fabrication and Processing of Nonferrous Metals,
General Research Institute for Nonferrous Metals, Beijing 100088, China;

2. College of Materials Science and Engineering, Chongqing University, Chongqing 400045, China;

3. National Research Center for Magnesium Alloys, Chongqing University, Chongqing 400044, China;

4. Creative Distribution Automation Co., Ltd., Beijing 100085, China

Received 28 November 2011; accepted 31 December 2012

Abstract: The effect of cold plastic deformation between solution treatment and artificial aging on the age-hardening response and mechanical properties of alloy was investigated by micro-hardness test, tensile test, optical microscopy (OM) and TEM observation. After solution treatment at 420 °C for 1 h, three kinds of pre-deformation strains, i.e. 0, 5% and 10%, were applied to extruded ZM61 bars. Age-hardening curves show that pre-deformation can significantly accelerate the precipitation kinetics and increase peak-hardness value; however, as pre-deformation strain rises from 5% to 10%, there is no gain in peak hardness value. The room temperature (RT) tensile properties demonstrate that increasing the pre-deformation degree can enhance the yield strength (YS) and ultimate tensile strength (UTS) but moderately reduce elongation (EL); furthermore, the enhancement of YS is larger than that of UTS. No twin can be observed in 5% pre-deformed microstructure; however, a large number of twins are activated after 10% pre-deformation. The peak-aged TEM microstructure shows that pre-deformation can increase the number density of rod-shaped β_1' precipitates which play a key role in strengthening ZM61 alloy.

Key words: Mg–6%Zn–1%Mn (ZM61); pre-deformation; age-hardening response; mechanical properties

1 Introduction

By thermal forming methods such as extrusion, rolling and forging, wrought magnesium alloys gain a refined microstructure including a very minor amount of pores, thin grains and uniform composition. Thus, compared to cast Mg alloys, wrought Mg alloys have homogeneous mechanical properties, largely improved ductility, high-level strength and high damage tolerance [1]. The low-cost high-strength Mg–6%Zn–1%Mn (ZM61) alloy is a good choice as wrought Mg alloy, since it can be smoothly extruded at 300–330 °C with full dynamic recrystallization (ultimate tensile strength (UTS) 305 MPa, yield strength (YS) 209 MPa and elongation (EL) 12% in as-extruded state) [2]. The mechanical properties of extruded ZM61 after T6

treatment of (420 °C, 2 h)+water quenching+(180 °C, 16 h) are: UTS=352 MPa, YS=314 MPa and EL=8%, which can match up to those of costly ZK60 alloy after T5 treatment, i.e., UTS=360 MPa, YS=295 MPa and EL=12% [2,3]. Such a pronounced strength increase in ZM61 alloy results from precipitate formation, and there are three kinds of precipitates in the peak-aged microstructure, i.e., predominant rod-like β_1' phases with their long axes parallel to $[0001]_{Mg}$ direction, a small number of disc-like β_2' phases lying flat on $(0001)_{Mg}$ plane and occasionally-observed polygon- or rod-like α -Mn particles [4–8]. Most researchers have acknowledged that both β_1' and β_2' are Laves phase $MgZn_2$ with a hexagonal structure ($a=0.520$ nm, $c=0.857$ nm) [9,10]; however, in several up-to-date literatures it is found that β_1' phase is Mg_4Zn_7 with a base-centered monoclinic structure ($a=2.596$ nm, $b=1.428$ nm, $c=0.524$

Foundation item: Project (2007CB613700) supported by the National Basic Research Program of China; Project (50725413) supported by the National Natural Science Foundation of China; Project (CDJXS11132228) supported by the Fundamental Research Funds for the Central Universities, China; Projects (2010DFR50010, 2008DFR50040) supported by International Cooperation Program, China; Projects (CSTC2009AB4008, 2010CSTC-HDLS) supported by Chongqing Sci & Tech Program, China

Corresponding author: Guo-liang SHI; Tel: +86-10-82241163; E-mail: sglholo@yahoo.com.cn

DOI: 10.1016/S1003-6326(13)62503-0

nm, $\gamma=102.5^\circ$) [5,11]. Figure 1(a) schematically shows the orientations of β_1' and β_2' in a hexagonal close-packed (HCP) α -Mg lattice and the realistic orientation is demonstrated in Fig. 1(b) which is a TEM bright-field image of T6-treated ZM61 alloy viewed along $[2\bar{1}\bar{1}0]_{\alpha\text{-Mg}}$. α -Mn particles with base-centered cubic (BCC) structure ($a=0.89125$ nm) are precipitated during high-temperature processes such as homogenization treatment, solution treatment or thermal deformation [7,8]. During hot forming, α -Mn precipitates can effectively hinder the growth of small recrystallized grains [12]. As shown in Fig. 1, compared to β_2' discs, β_1' rods can more seriously impede the dislocation glide on basal plane which is the dominant deformation mode at temperatures lower than 250 °C [13]. Consequently, β_1' rods are the main cause of precipitation strengthening and widespread β_2' discs bring about over-aging [10], implying that strengthening effect can be further enhanced by means of increasing the number density of

β_1' rods. Generally, micro-alloying, double aging and cold deformation prior to aging can increase the number density of precipitates [14]. However, in the case of Mg alloys, rare attention has been paid to pre-deformation prior to aging. High-density dislocations and twin boundaries, formed during cold pre-deformation, can provide a large number of heterogeneous nucleation sites and dense dislocations can also act as quick diffusion pipes, resulting in increased precipitate number density and also accelerated precipitation kinetics [15,16].

The present work explores the role of cold pre-deformation on the age-hardening response and mechanical properties of Mg–6%Zn–1%Mn alloy, aiming to further elevating the yield strength of this low-cost alloy and thus broadening its application field.

2 Experimental

Ingot with the nominal composition of Mg–6%Zn–1%Mn was prepared by semi-continuous casting. Melting was conducted in an electrical resistance furnace and a molten-salt flux composed of MgCl_2 , KCl, CaF_2 and BaCl_2 was used for covering and refining. After pure Mg ingots had wholly melted at 880 °C in a bottom-pour iron crucible, heating was stopped and Mg–4.2%Mn master alloy was added as the temperature fell to 800 °C and then pure Zn ingot was added as the temperature dropped to 720 °C. The alloy melt was reheated to 760 °C, followed by skimming, stirring, refining and holding for 20 min. Finally, heating was ceased and the melt was poured into a semi-continuous crystallizer under an inert atmosphere of CO_2 and SF_6 mixture when the temperature fell to about 730 °C. The chemical composition was Mg–5.77%Zn–0.94%Mn, which was measured by a Shimadzu XRF–1800CCDE X-ray fluorescence spectrometer. The ingot was then worked into extrusion billets ($d80$ mm \times 250 mm). After a two-step homogenization treatment, i.e., (330 °C, 8 h)+(420 °C, 2 h), these billets were extruded at 320 °C immediately. The extrusion parameters are listed in Table 1. Three segments ($d16$ mm \times 250 mm) were annealed at 420 °C for 1 h followed by water quenching and then two of them were machined into dog-bone shape (with $d13$ mm gauge diameter and 200 mm gauge length) for RT stretch pre-deformation. Two kinds of plastic tensile strains, 5% and 10%, were used. Samples cut from the pre-deformed and non-pre-deformed segments were subjected to artificial aging at 180 °C to achieve age-hardening curves. Vickers hardness was measured under a load of 0.49 N and a holding time of 20 s, and each hardness value was the average of 20 data. Both pre-deformation and tensile test were conducted on a Sans CMT–5105 electronic universal testing machine with a strain rate of 3 mm/min, and the dimensions of

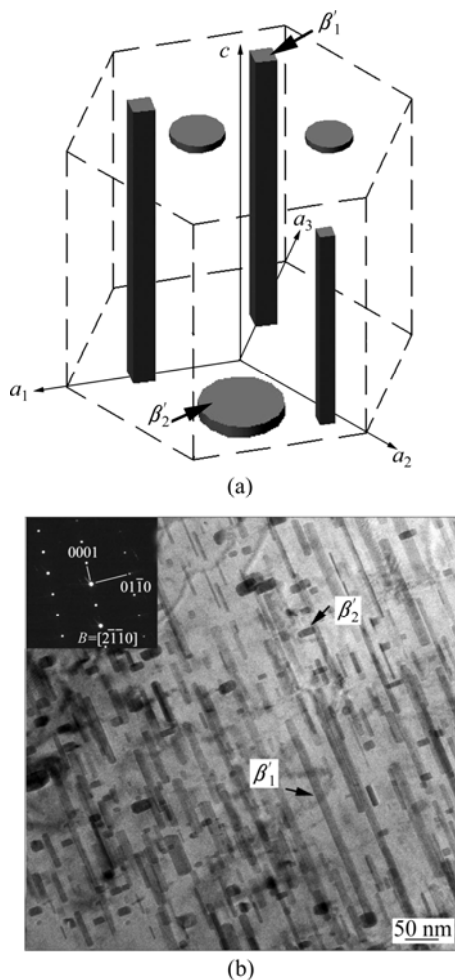


Fig. 1 Orientation of β_1' and β_2' in HCP α -Mg matrix: (a) A schematic diagram showing β_1' rods and β_2' discs in a α -Mg unit cell; (b) TEM bright-field image of T6-treated ZM61 alloy ((420 °C, 1 h)+water quenching+(180 °C, 9 h)) viewed along $[2\bar{1}\bar{1}0]_{\alpha\text{-Mg}}$ (achieved from the present work)

dog-bone specimens for tensile test were $d5$ mm gauge diameter and 50 mm gauge length. TEM observation was performed on a Zeiss LIBRA 200 FE TEM under an accelerating voltage of 200 kV. Thin foil specimens were cut from hardness-test samples and prepared by the twin-jet polishing technique in a solution of 5.3 g LiCl, 11.16 g $Mg(ClO_4)_2$, 500 mL methanol and 100 mL 2-butoxy-ethanol at -50 °C and 90 V. Small-angle ion milling was utilized to remove oxide films and contaminations on the two surfaces of perforated specimens.

Table 1 Extrusion parameters of ZM61 Mg alloys

Temperature/°C		Extrusion speed/ (m·min ⁻¹)	Extrusion ratio	Cooling-Down method	
Billet	Mould				
320	320	320	2	25	Air cooling

3 Results

3.1 Age-hardening curves

The age-hardening curves of ZM61 samples with three kinds of pre-deformation strains, i.e. 0, 5% and 10%, are illustrated in Fig. 2, and some key characteristic parameters are listed in Table 2. It can be seen that cold pre-deformation brings out four phenomena. Firstly, the initial hardness values show a linear increase with the increment of pre-deformation strain, indicating that the pre-deformation brings about serious work hardening effect in textured ZM61 alloy. Secondly, as pre-deformation level increases, time needed to reach peak hardness can be exponentially shortened. Only 0.8 h is needed for 10% strained sample to reach peak hardness compared to 9 h for unstrained one and 4 h for 5% strained one. Thirdly, as pre-deformation strain rises from 0 to 5%, peak hardness value increases from HV 81 to HV 88; however, the peak hardness value of 10% strained sample stays at the same level as that of 5%

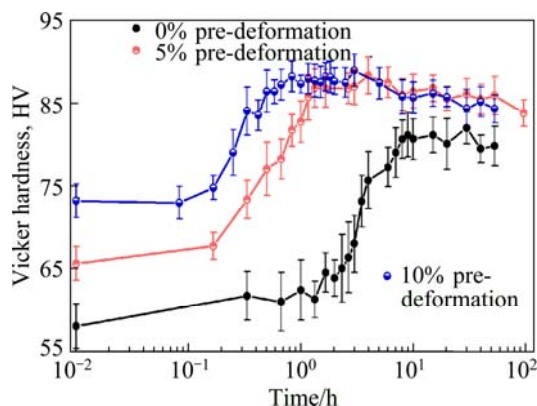


Fig. 2 Age-hardening curves of ZM61 specimens with 0, 5% and 10% pre-deformation strain at 180 °C

Table 2 Some key characteristic parameters of age-hardening curves in Fig. 2

Pre-deformation strain	Initial hardness value (HV)	Peak hardness value (HV)	Time needed to reach peak hardness/h	Maximum hardness increment (HV)
0	58	81	9	23
5%	66	88	4	22
10%	73	88	0.8	15

strained one. Finally, the maximum hardness increment tends to reduce with the rise in pre-deformation strain.

3.2 Mechanical property

In order to get peak-aging mechanical properties, based on age-hardening curves in Fig. 2, 9, 5 and 3 h were selected as aging time for 0, 5% and 10% stretched samples, respectively. The RT stress—strain curves of the peak-aged samples are shown in Fig. 3, which also include the curve of as-extruded sample for comparing, and the mechanical properties are listed in Table 3. Compared with the as-extruded sample, the peak aged ones gain substantial increment in YS and UTS but their elongation is largely degraded. On the other hand, with

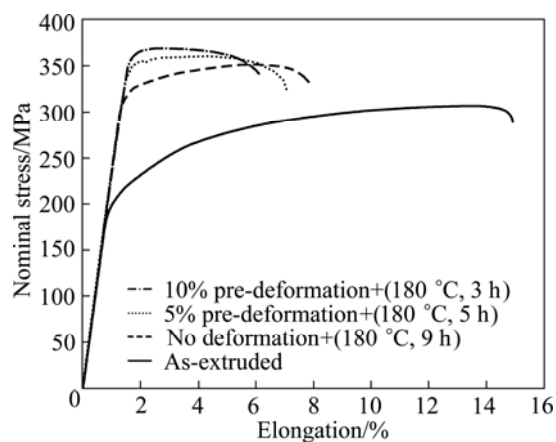


Fig. 3 RT stress—strain curves of as-extruded sample and peak-aged ones with 0, 5% and 10% pre-deformation strain

Table 3 RT mechanical properties of as-extruded and peak-aged ZM61 samples

Condition	YS/MPa	UTS/MPa	Elongation/%
As-extruded	204	306	14
Solution treatment+(180 °C, 9 h)	320	350	6
Solution treatment+5% pre-deformation strain+(180 °C, 5 h)	347	360	6
Solution treatment+10% pre-deformation strain+(180 °C, 3 h)	356	366	4

the rise in pre-deformation level, the strength of the peak aged sample increases, YS in particular, whereas the elongation tends to decrease. As tensile strain rises from 0 to 5%, the YS gains an 8.4% increase with minor loss in elongation; however, from 5% to 10%, the YS gains a 2.5% increase with a 28% loss in elongation, indicating that further pre-deformation after 5% only brings trivial increase in strength but significantly lowers the elongation.

3.3 Microstructure

Figure 4 shows the optical images of as-extruded and as-annealed microstructure. After hot extrusion at 320 °C, dynamic recrystallization has occurred, resulting in an average grain size of about 10 μm (Fig. 4 (a)), and minor second-phase particles (streams) are retained, indicating that two-step homogenization treatment before extrusion can effectively dissolve the interdendritic compounds. Normal grain growth and dissolution of the retained second-phase particles take place during solution treatment at 420 °C for 1 h, resulting in an average grain size of about 20 μm.

Figure 5 shows optical images of 5% and 10% pre-deformed microstructures. It is notable that almost no twin can be observed in 5% pre-deformed microstructure. When cold pre-deformation strain rises to 10%, most of the larger grains contain twins (Figs. 5(c) and (d)).

Figure 6 shows the peak-aged TEM microstructure of pre-deformed and non-pre-deformed ZM61 samples.

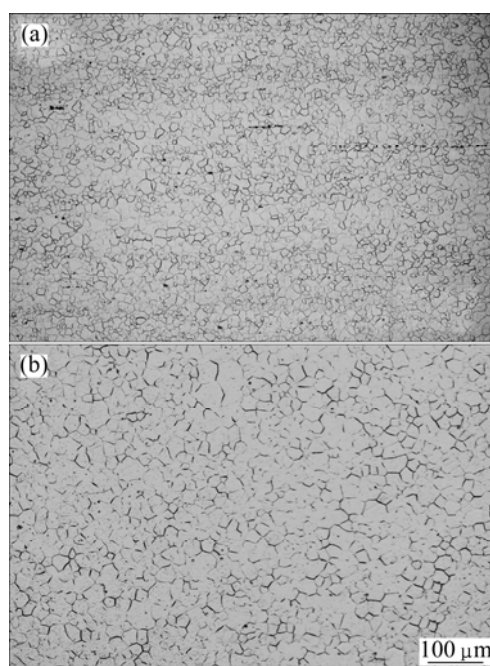


Fig. 4 Optical images of as-extruded (a) and as-annealed (b) ZM61 alloy

Since the observation directions are all near $[0001]_{Mg}$, rod-shaped β_1' precipitates with their long axes parallel to $[0001]_{Mg}$ become particles and thus such observation direction favors the determination of their number density. It can be seen that the number density of β_1' phase is significantly increased with the rise in pre-

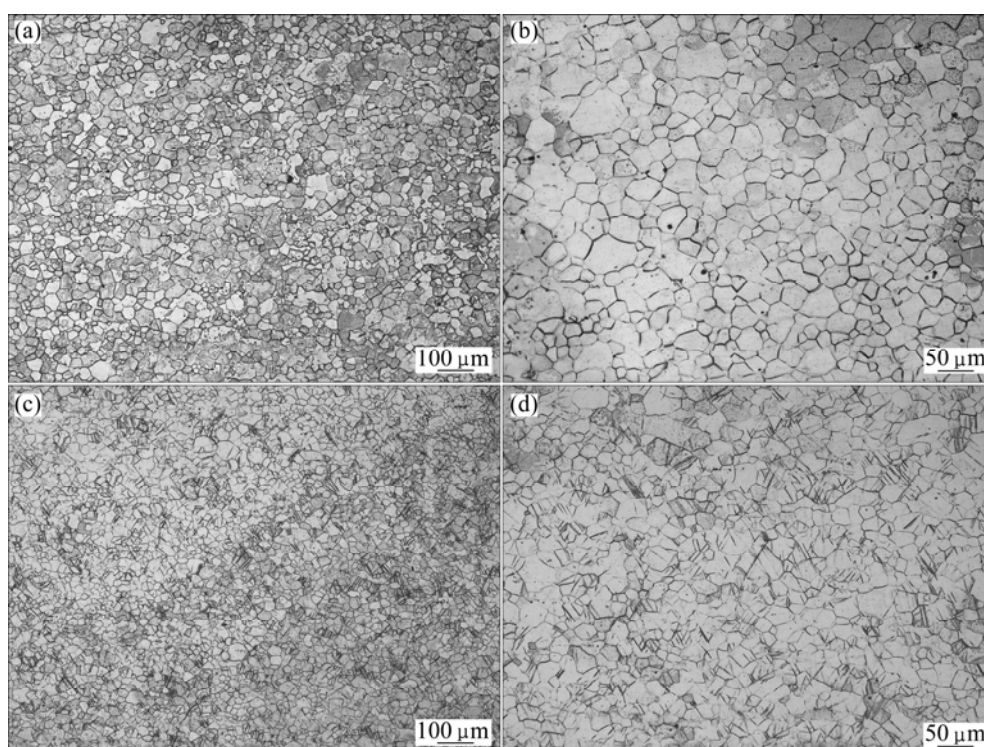


Fig. 5 Optical images of cold-deformed ZM61 alloy with extrusion direction (or cold pre-deformation axis) parallel to each scale bar: (a), (b) 5% pre-deformation strain; (c), (d) 10% pre-deformation strain

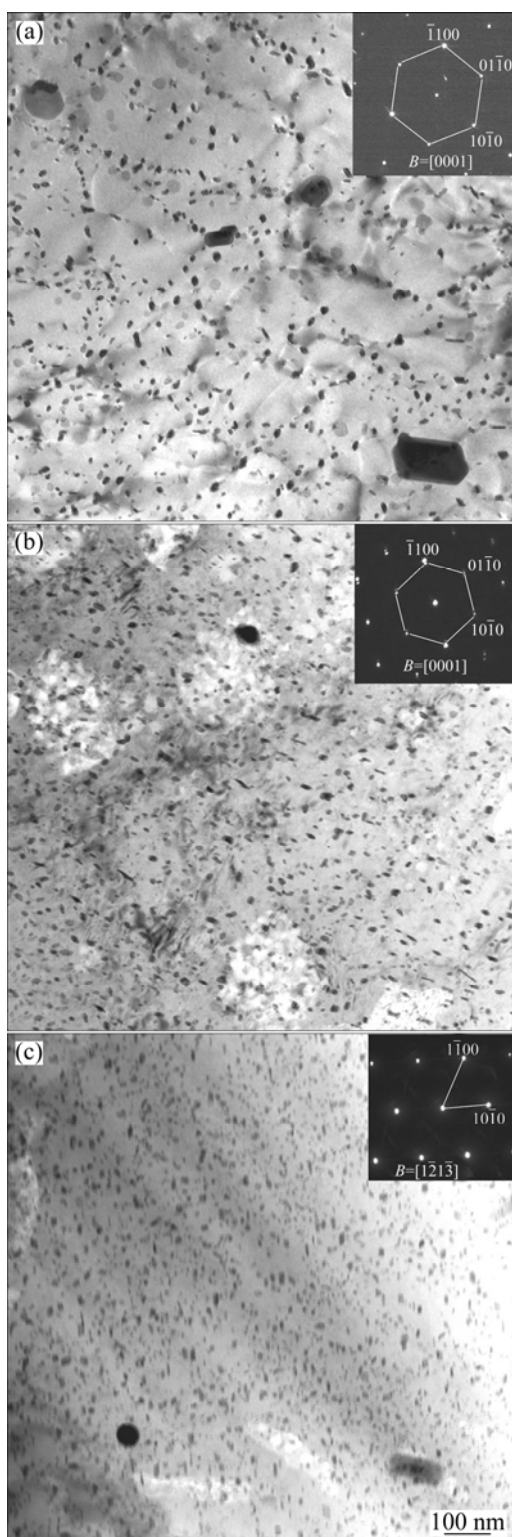


Fig. 6 TEM bright field images of peak-aged samples with different pre-deformation strains: (a) 0%, (180 °C, 9 h); (b) 5%, (180 °C, 4 h); (c) 10%, (180 °C, 0.8 h)

deformation level. It is noteworthy that β_1' rods are aligned in lines even in non-pre-deformed sample, which is most likely caused by heterogeneous nucleation on equilibrium state dislocations, indicating that dislocation is a preferred nucleation site for β_1' phase.

4 Discussion

First of all, the microstructure evolution during hot-extrusion, solution treatment, pre-deformation and aging should be understood. A complete-dynamic-recrystallization microstructure has been built up in ZM61 alloy after hot extrusion at 320 °C, resulting in an average grain size of about 10 μm , as shown in Fig. 4(a). Moreover, an intensive basal texture also arises after hot extrusion, that is, the (0001) basal planes of most grains are parallel to extrusion direction [17,18]. During the solution treatment, normal grain growth, dissolution of second-phase particle and dislocation recovery take place, and the average grain size after solution treatment is about 20 μm , as shown in Fig. 4(b). It has been reported that moderate annealing after deformation only brings about trivial change in the texture in HCP metals [19], so the basal texture can be maintained after solution treatment. During the cold stretch along extrusion direction, the c -axes of most grains are perpendicular to tensile load direction because of the basal texture, so it is very hard to activate the basal slip system since its Schmid factor is near zero. In such case, non-basal-plane slipping and contraction twinning will be activated in most grains [20–22]. It is worth to note that non-basal dislocations are firstly activated before twinning, as shown in Fig. 5, since twinning becomes increasingly difficult with decreasing grain size [22]. With the rise in pre-deformation strain, the number of dislocations and twins will be considerably increased, which can be known from the linear increase in initial hardness values, as can be seen in Fig. 2 and Table 2. During the aging, high density dislocations gradually recover [23] and a large number of β_1' rods heterogeneously nucleate on the dislocations and twin boundaries. The dislocation segments where precipitates are selected as nucleation sites will be annihilated, thus one continuous dislocation will turn into interrupted segments [16], so the peak-aged microstructure includes vast amounts of heterogeneously nucleated β_1' rods, dense dislocation segments and numerous twins.

In this study, the influence of cold pre-deformation on the age-hardening response and mechanical properties can be summarized in four parts: 1) pre-deformation brings about marked work hardening effect; 2) rise in pre-deformation strain can significantly speed up the age-hardening kinetics; 3) the YS gains notable elevation as pre-deformation strain increases; 4) when pre-deformation strain rises from 5% to 10%, the peak hardness value gains no increment. The initial hardness values of 0, 5% and 10% strained samples are HV 58, HV 66 and HV 73, respectively. Such effective work hardening response is attributed to numerous twins and

high-density dislocations formed during cold pre-deformation. ZHENG et al [16] reported an investigation similar to the present work, and in their work the work-hardening response brought out by cold stretching in an Mg–Gd–Nd–Zr alloy is much weaker than that in the present work. Their alloy must be texture-free since no hot-deformation was applied, indicating that texture has an important influence on the total amount of twins and dislocations formed during the cold pre-deformation. In random orientated alloy, basal plane slip takes a high proportion during cold deformation; by contrast, in the present case, a large number of non-basal dislocations are activated first and they become immobile gradually by the formation of many jogs on them during the motion [24], resulting in a huge increase in dislocation density and thus an enhanced work-hardening effect. Besides acting as nucleation sites, dislocations can also act as fast diffusion pipes for solute Zn, so the presence of high density dislocations will considerably speed up the precipitation rate of β_1' phase which is the key hardener of ZM61 alloy, that is why pre-deformation can severely enhance the age-hardening kinetics. The YS is very sensitive to the number density of precipitates, since the more the precipitates are, the shorter the distance between them is, thus, the more difficult the dislocations to bypass them is, resulting in a macroscopic rise in YS. Numerous twin boundaries and dislocations arising from cold pre-deformation boost the number density of β_1' rods, as shown in Fig. 6, so the YS rises with the increase in pre-deformation strain. There is an incredible phenomenon in this work, that is, after 5%, a further increase in pre-deformation strain brings about trivial increment in the peak-hardness value and YS. In the case of pre-deformed sample, two main factors, i.e. precipitation hardening and work hardening, determine the increment in peak-hardness value and YS; during the aging at 180 °C, the dislocation density will gradually reduce because of the recovery and it seems that severer pre-deformation level leads to severer recovery. Therefore, when pre-deformation strain reaches to 10%, the degradation in hardness and YS caused by severely weakened work-hardening effect can counteract their rise caused by enhanced precipitation hardening effect.

This work indicates that a small amount of cold-plastic-deformation can further raise YS of ZM61 alloy and also effectively shorten the peak-aging time, which can expand the application field of this low-cost alloy.

5 Conclusions

1) Cold pre-deformation brings about remarkable work-hardening effect in textured ZM61 alloy and also

considerably speeds up the age-hardening kinetics. As pre-deformation strain increases from 0 to 5%, the peak hardness value gains an obvious rise; however, it gains no rise as the strain increases from 5% to 10%.

2) As cold tensile strain rises from 0 to 5%, the peak-aging yield strength largely increases from 320 MPa to 347 MPa with minor deterioration in elongation; as the strain rises from 5% to 10%, the peak-aging yield strength achieves a minor increase from 347 MPa to 356 MPa with a large deterioration in elongation.

3) Almost no twinning occurs in 5% strained sample; however, a lot of twins are activated after 10% pre-deformation.

4) In the peak-aging microstructure, the number density of β_1' rods increases with the rise in pre-deformation level.

References

- [1] SEBASTIAN W, DRÖDER K, SCHUMANN S. Properties and processing of magnesium wrought products for automotive applications [C]//KAINER K U. Magnesium Alloys and Their Applications. Weinheim: Wiley-VCH, 2000: 602.
- [2] ZHANG Ding-fei, SHI Guo-liang, ZHAO Xia-bing, QI Fu-gang. Microstructure evolution and mechanical properties of Mg-x%Zn-1%Mn (x=4, 5, 6, 7, 8, 9) wrought magnesium alloys [J]. Transactions of Nonferrous Metals Society of China, 2011, 21: 15–25.
- [3] HABASHI F. Alloys: Preparation, properties, applications [M]. Weinheim: Wiley-VCH, 1998: 152.
- [4] CLARK J B. Transmission electron microscopy study of age hardening in a Mg–5wt.% Zn alloy [J]. Acta Metallurgica, 1965, 13: 1281–1289.
- [5] GAO X, NIE J F. Characterization of strengthening precipitate phases in a Mg–Zn alloy [J]. Scripta Materialia, 2007, 56: 645–648.
- [6] OH-ISHI K, HONO K, SHIN K S. Effect of pre-aging and Al addition on age-hardening and microstructure in Mg–6wt% Zn alloys [J]. Materials Science and Engineering A, 2008, 496: 425–433.
- [7] SKJERPE P M, SIMENSEN C J. Precipitation in Mg–Mn alloys [J]. Metal Science, 1983, 17: 403–407.
- [8] ZHANG M X, KELLY P M. Edge-to-edge matching and its applications: Part II. Application to Mg–Al, Mg–Y and Mg–Mn alloys [J]. Acta Materialia, 2005, 53: 1085–1096.
- [9] CHUN J S, BYRNE J G. Precipitate strengthening mechanisms in magnesium zinc alloy single crystals [J]. Journal of Materials Science, 1969, 4: 861–872.
- [10] WEI L Y, DUNLOP G L, WESTENGEN H. Precipitation hardening of Mg–Zn and Mg–Zn–RE alloys [J]. Metall Mater Trans A, 1995, 26: 1705–1716.
- [11] SINGH A, TSAI A P. Structural characteristics of precipitates in Mg–Zn-based alloys [J]. Scripta Materialia, 2007, 57: 941–944.
- [12] ROBSON J D, HENRY D T, DAVIS B. Particle effects on recrystallization in magnesium- manganese alloys: Particle pinning [J]. Materials Science and Engineering A, 2011, 528: 4239–4247.
- [13] GALIYEV A, KAIBYSHEV R, GOTTSTEIN G. Correlation of plastic deformation and dynamic recrystallization in magnesium alloy ZK60 [J]. Acta Materialia, 2001, 49: 1199–1207.
- [14] NIE J F. Effects of precipitate shape and orientation on dispersion strengthening in magnesium alloys [J]. Scripta Materialia, 2003, 48: 1009–1015.
- [15] PORTER D A, EASTERLING K E. Phase transformations in metals

- and alloys [M]. London: Chapman & Hall, 1992.
- [16] ZHENG K Y, DONG J, ZENG X Q, DING W J. Effect of pre-deformation on aging characteristics and mechanical properties of a Mg–Gd–Nd–Zr alloy [J]. *Materials Science and Engineering A*, 2008, 491: 103–109.
- [17] LASER T, HARTIG C, NÜRNBERG M R, LETZIG D, BORMANN R. The influence of calcium and cerium mischmetal on the microstructural evolution of Mg–3Al–1Zn during extrusion and resulting mechanical properties [J]. *Acta Materialia*, 2008, 56: 2791–2798.
- [18] WANG Y N, HUANG J C. The role of twinning and untwinning in yielding behavior in hot-extruded Mg–Al–Zn alloy [J]. *Acta Materialia*, 2007, 55: 897–905.
- [19] PÉREZ-PRADO M T, RUANO O A. Texture evolution during grain growth in annealed MG AZ61 alloy [J]. *Scripta Materialia*, 2003, 48: 59–64.
- [20] KESHAVARZ Z, BARNETT M R. EBSD analysis of deformation modes in Mg–3Al–1Zn [J]. *Scripta Materialia*, 2006, 55: 915–918.
- [21] CIZEK P, BARNETT M R. Characteristics of the contraction twins formed close to the fracture surface in Mg–3Al–1Zn alloy deformed in tension [J]. *Scripta Materialia*, 2008, 59: 959–962.
- [22] KOIKE J, KOBAYASHI T, MUKAI T, WATANABE H, SUZUKI M, MARUYAMA K, HIGASHI K. The activity of non-basal slip systems and dynamic recovery at room temperature in fine-grained AZ31B magnesium alloys [J]. *Acta Materialia*, 2003, 51: 2055–2065.
- [23] ČÍŽEK J, PROCHÁZKA I, SMOLA B, STULÍKOVÁ I, OČENÁŠEK V. Influence of deformation on precipitation process in Mg–15wt.%Gd alloy [J]. *Journal of Alloys and Compounds*, 2007, 430: 92–96.
- [24] YOSHINAGA H, HORIUCHI R. On the nonbasal slip in magnesium crystals [J]. *Transactions of the Japan Institute of Metals*, 1964, 5: 12–21.

预变形对挤压态 Mg–6%Zn–1%Mn 镁合金 时效硬化效应和力学性能的影响

石国梁¹, 张丁非^{2,3}, 张红菊², 赵霞兵⁴, 齐福刚², 张奎¹

1. 北京有色金属研究总院 有色金属材料制备加工国家重点实验室, 北京 100088;
2. 重庆大学 材料科学与工程学院, 重庆 400045;
3. 重庆大学 国家镁合金材料工程技术研究中心, 重庆 400045;
4. 北京科锐配电自动化股份有限公司, 北京 100085

摘要: 采用显微硬度测试、拉伸试验、金相观察和 TEM 观察, 研究冷塑性变形对 Mg–6%Zn–1%Mn (ZM61) 合金时效硬化和力学性能的影响。在 420 °C 固溶处理 1 h 后, 对 ZM61 挤压棒材试样进行室温拉伸变形, 塑性应变有 3 种: 0、5% 和 10%, 预变形后再进行人工时效。时效硬化曲线表明: 预变形可以显著加快硬化速率且提高峰值硬度; 然而, 当应变量由 5% 增加到 10% 后, 峰值硬度并未增加。室温拉伸性能表明: 预变形量增加, 屈服强度和抗拉强度增加, 伸长率略有降低, 且屈服强度的增加幅度大于抗拉强度的。金相组织观察表明: 当预变形应变量为 5% 时, 金相组织中未观察到孪晶; 预变形 10% 的组织中出现了大量的孪晶。TEM 观察表明: 预变形可以增加峰时效态组织中 β_1' 杆状相的数量。

关键词: Mg–6%Zn–1%Mn (ZM61); 预变形; 时效硬化效应; 力学性能

(Edited by Hua YANG)